Cellulose interactions with CO<inf>2</inf> in NaOH(aq): The (un)expected coagulation creates potential in cellulose technology

Carbohydrate Polymers 294 (2022) 119771

Contents lists available at ScienceDirect

Carbohydrate Polymers

journal homepage: www.elsevier.com/locate/carbpol

Cellulose interactions with CO_2 in NaOH(aq): The (un)expected coagulation creates potential in cellulose technology

Aleksandra M. Kozlowski [a], Merima Hasani [a,b,*]

[a] Division of Forest Products and Chemical Engineering, Department of Chemistry and Chemical Engineering, Chalmers University of Technology, SE-412 96 Göteborg, Sweden

[b] Wallenberg Wood Science Center, Chalmers University of Technology, SE-412 96 Gothenburg, Sweden

ARTICLE INFO

Keywords:
Cellulose/NaOH(aq) solution
CO_2(g) chemisorption
CO_2(g) coagulant
In-situ FTIR

ABSTRACT

Upon the search for a suitable processing method for cellulose, the dissolution in NaOH(aq) presents a real green potential, including its ability to sorb environmental CO_2(g) affecting dissolution. Here, CO_2(g) was delivered in a controlled way to the cellulose/NaOH(aq) system during the *in-situ* analysis with FTIR, pH and temperature meters, resulting in efficient coagulation of cellulose. Surprisingly, the coagulation occurred with a minimal loss of alkalinity. This was considered an effect of a specific interaction between the dissolved polymer and gas, resulting in the introduction of carbonate species, highly influential in the coagulation process. The process repeated at 25 °C and 5 °C suggested a strong influence of temperature. The conversion routes of the CO_2(g) coagulant were also related to the dissolved state of the polymer. The recovered cellulose appeared competitive with EtOH recovery in terms of structure. The presented finding put a perspective on the utilisation of both the coagulation process and final materials in cellulose technology.

1. Introduction

The increasing environmental crisis brought the attention of governments, industries and finally the customers towards sustainable materials, carrying the renewable and biodegradable potential. In this context cellulose, the fundamental component of plant cell walls with a range of structural levels is attractive as a versatile biomaterial platform for multiple applications. Cellulose has an extremely stable molecular structure, being a combination of rigid 1,4-glycosidic bonds between the 180° inverted β-D-glucose units and the hydrogen bonding of the equatorially placed hydroxyl groups. These allow the assembly of adjacent chains in an extended sheet framework, stacking further into a crystalline structure, primarily through van der Waals interactions, sporadically interrupted by the less ordered regions (Medronho and Lindman, 2015; O'sullvian, 1997).

Given the poor melting properties, reshaping cellulose through dissolution is a crucial non-destructive processing tool for a range of applications, including the critical efforts on recycling textile waste. Consequently, the subject of a successful cellulose solvent, which will prove right from a sustainable perspective, remains an active research area; especially since poor cellulose solubility poses a scientific and processing challenge. In this respect, the aqueous hydroxide bases with a lead of the cheap, non-toxic and widely used NaOH(aq) are particularly attractive. Unfortunately, the dissolution scope of cellulose in NaOH(aq) is limited both in terms of the dissolution conditions (low temperature and a narrow base concentration range of 7–10 %) and concerning cellulose substrate character (Budtova and Navard, 2016; Cuissinat and Navard, 2008; Egal et al., 2007). The poor solubility has, among the other factors, been attributed to the abovementioned amphiphilicity along with a peculiar supramolecular and morphological arrangement (Bergenstråhle et al., 2010; Lindman et al., 2010; Zhang et al., 2002), while the role of cellulose deprotonation (logically possible at such high pH), as well as the cation and ion-dipole interactions, are the subjects of ongoing discussion (Budtova and Navard, 2016; Lindman et al., 2017; Swensson et al., 2020).

Besides the aspects associated with cellulose, the performance of the solvent is crucial for a successful process. However, it seems that in the case of NaOH(aq) the discussion has been systematically limited to the effect of base concentration and hydration, avoiding the subject of its natural ability to bind environmental CO_2(g). The CO_2(g) intake by NaOH(aq) has been studied since the early 1940s (Darmana et al., 2007; Fleischer et al., 1996; Hikita et al., 1976; Tepe and Dodge, 1943). It is either seen as a disadvantage (*i.e.:* stability and use of concentrated NaOH) (Benedetti-Pichler et al., 1939; Schönherr et al., 2018; Sipos

* Corresponding author at: Department of Chemistry and Chemical Engineering, Chalmers University of Technology, Kemigården 4, 412 96 Göteborg, Sweden.
E-mail addresses: aleksandra.kozlowski@chalmers.se (A.M. Kozlowski), merima.hasani@chalmers.se (M. Hasani).

https://doi.org/10.1016/j.carbpol.2022.119771
Received 30 May 2022; Received in revised form 18 June 2022; Accepted 20 June 2022
Available online 26 June 2022

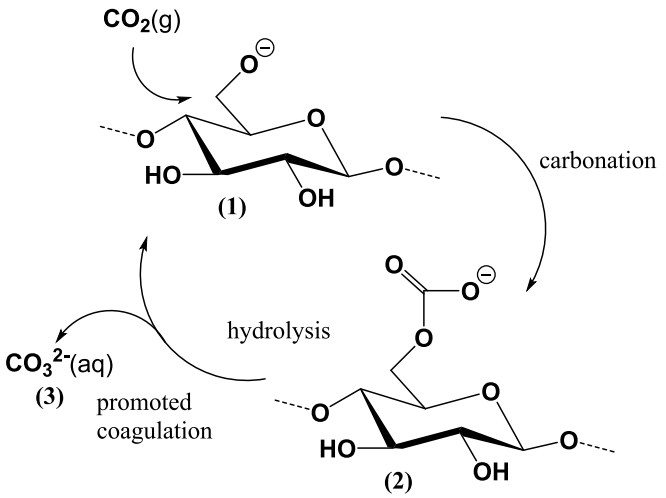

Scheme 1. Proposed chemisorption mechanism of CO_2(g) by dissolved, partly deprotonated cellulose (1) going through formation of a transient cellulose carbonate (2) and a subsequent hydrolysis forming CO_3^{2-} (3), promoting coagulation.

et al., 2000) or as an asset in specific treatments (*e.g.* precipitation of carbonated salts) (Adnan et al., 2020; Goharrizi and Abolpour, 2014; Saberi et al., 2009); one way or the other, it is acknowledged. Unfortunately, until recently, that has not been a case for studies involving cellulose in NaOH(aq).

The results of previous research carried out by our group showed that cellulose exhibits a strong affinity for alkali-dissolved CO_2(g), most probably forming a cellulose carbonate intermediate that could be the reason for the limited dissolution and stability of cellulose in NaOH(aq) (Gunnarsson et al., 2017, 2018, 2020; Gunnarsson et al., 2021a; Gunnarsson et al., 2021b). Following the previous studies, we continue to investigate the complex relationship between cellulose, NaOH(aq) and CO_2(g) from a broader perspective. Upon the earlier discovered cellulose-mediated chemisorption of CO_2(g) into the NaOH(aq), here we hypothesise a coagulant activity of the introduced CO_2(g). To minimize the effect of spontaneous coagulation in alkali that could be triggered by the insufficient dissolution of the polymer, the microcrystalline cellulose of relatively low degree of polymerization is dissolved at a concentration previously proven as effective (Egal et al., 2008; Roy et al., 2001). This strategy allows us to fully understand the effect of CO_2 (g) on studied material. With the chemisorption likely relying on the reaction of CO_2(g) with cellulose alkoxides (not OH^-) (Scheme 1), the coagulation is expected to proceed under only modest alkalinity loss, opening for efficient recycling facilitating implementation. To investigate the coagulation mechanism and its dependency on applied conditions, the process was followed through *in-situ* measurements (FTIR, pH, temperature). From the practical perspective, the presented process could be foreseen as potential in further technological applications like cellulose regeneration. Therefore, the obtained CO_2-precipitates were structurally investigated and compared with the material precipitated with EtOH. From the theoretical perspective, the presented article gives additional insight into the chemisorption of CO_2(g) by the cellulose-NaOH(aq) and contributes to the understanding of the interaction mechanism.

2. Experimental

2.1. Materials

All reagents used were of analytical grade or higher. All solutions were prepared in ultrapure water (up H2O) of resistivity ≥18.2 MΩ.cm/25 °C (Direct-Q, Millipore). Extra pure sodium hydroxide (50 % wt aq.) and absolute ethanol (≥99.96 %, EtOH) were purchased from VWR (Fontenay-sous-Bois, France). Avicel PH-101 microcrystalline cellulose (MCC, ~50 μm particle size, FMC Corp.), with a degree of polymerization of ~230, was purchased from Sigma-Aldrich (now Merck, Darmstadt, Germany). Nitrogen (≥99.996 %) and carbon dioxide gases were provided by Linde (Göteborg, Sweden).

2.2. The interaction between CO_2(g) and aqueous solutions

2.2.1. The experimental set-up

The illustrative scheme of the experimental set-up, including *in-situ* measuring probes, is presented in Fig. 1. The studies of the interaction between CO_2(g) and NaOH(aq) and cellulose/NaOH(aq) were carried out in a borosilicate reaction vessel (150 ml), covered with a 5-openings lid with an FPM seal (Methrom AG, Herisau, Switzerland) and connected to a pressurized gas tank *via* a glass variable area flowmeter (1–12 × l/min, Platon, Saint Etienne, France). Gasses (N_2 or CO_2) were delivered through a glass inlet with a PTFE tip (⌀ = 0.86 mm), secured by an overflow tube and a valve (Methrom AG, Herisau, Switzerland). For the experiment carried out at 5 °C, the system was cooled in the iced water bath; for the experiment carried out at 25 °C the vessel was placed in a water bath to sustain constant conditions. The temperature outside the vessel was controlled with a thermocouple thermometer (Dual J-E-T-K, Barnant, USA). The pH and inner temperature of the solutions were *in-situ* measured with a combination electrode (IntelliCAL™, PHC705A) connected to a laboratory multimeter (HQ430D, Hatch, Düsseldorf, Germany). The IR spectra were *in-situ* collected with an ATR probe (DS AgX Comp ™) connected to an FTIR spectrometer (ReactIR 702L, Metler Toledo, Stockholm, Sweden).

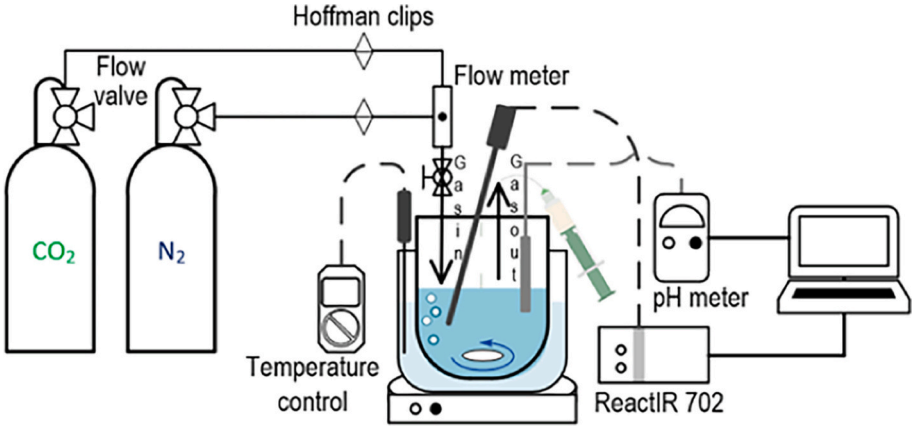

Fig. 1. The set-up was applied in the CO_2-chemisorption experiment.

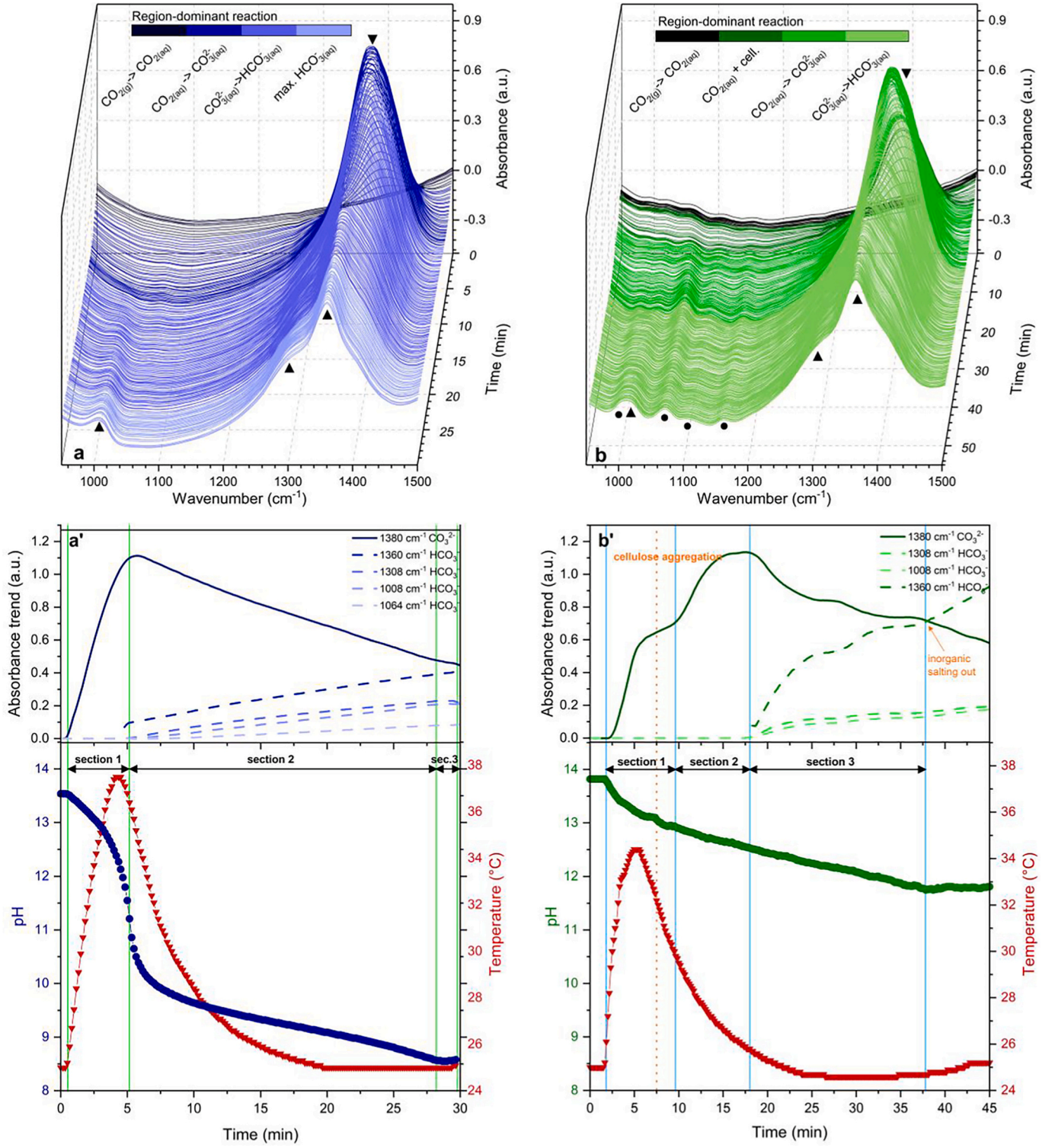

Fig. 2. The FTIR absorbance of carbonate ions, change of pH and temperature, observed during the sparging of CO_2(g) over the a) 2.0 M NaOH and b) cellulose/2.0 M NaOH(aq) at 25 °C. Aggregation of cellulose and inorganic salting-out were marked with orange. ▼ – CO_3^{2-} peaks; ▲ – HCO_3^- peaks. ● – cellulose peaks.

2.2.2. *Study of the reaction between CO_2(g) and NaOH(aq)*

The solution of 2.0 M NaOH(aq) (50 ml) was prepared from a concentrated stock directly in the reaction vessel while sparging with N_2 for 15 min, at a constant flow of 0.5 l/min, to minimize the influence of the environmental CO_2. Thereafter, the vessel valves were shut, and the nitrogen tank was replaced with carbon dioxide. The solvent was continuously sparged with CO_2 at 1.5 l/min. To minimize the loss of CO_2 from the absorber and for a homogeneous reaction, the stirrer was rotated at a low speed of 50 rpm (Benedetti-Pichler et al., 1939). The process was timed; the pH and temperature variations were measured at 10 s intervals until the natural endpoint, that is until the precipitation of carbonated sodium salt(s) (Bonfim-Rocha et al., 2020; Shim et al., 2016).

2.2.3. *Study of the reaction between CO_2 and cellulose-NaOH (aq)*

The procedure was repeated for the cellulose/NaOH/(aq) system

(2.0 % in 2.0 M, respectively) prepared in the reaction vessel before CO_2 injection. To avoid clustering of cellulose, the MCC was initially dispersed in ultrapure water and cooled down in an ice bath. The cold dispersion (0.5 °C) and a pre-cooled, concentrated NaOH (10 °C) were both sparged with N_2 (15 min, 0.5 l/min) and combined under an increased flow of N_2, to minimize the absorption of atmospheric CO_2. The reaction vessel was placed in an isothermal container with a minimal amount of dry ice, so the solution temperature decreased to −7 °C (±1 °C). The system was kept under N_2 flow for 1 h with vigorous stirring. The dissolution status was assessed with Discovery.V12 stereomicroscope (ZEISS, Oberkochen, Germany).

For the CO_2 experiment carried out at 25 °C, the vessel with the dissolved MCC was equilibrated at room temperature and afterwards placed in the water bath. For the experiment carried out at 5 °C, the vessel was placed directly in the iced-water bath. The temperature equilibration was carried under an N_2 atmosphere with stirring. Thereafter, the CO_2 sparging was repeated following the protocol described above. The gels precipitated upon the gas sparging were further analysed.

2.3. Treatment and analysis of generated cellulose gels

2.3.1. Washing and drying

The generated cellulose precipitates were washed with up H_2O under the vacuum on Büchner funnels with binder-free glass microfiber filters (Cytiva Whatman™) and either freeze-dried for at least 48 h (NMR analysis) or initially air-dried followed by drying at 35 °C for 48 h (XRD and FTIR analysis). For reference, the NaOH(aq) dissolved cellulose (same dissolution approach as described in Section 2.2.3) was precipitated with absolute EtOH with an identical washing and drying procedure, similar to the MCC reference standard.

2.3.2. NMR spectroscopy

The samples (30 mg) were dissolved in 0.6 ml of DMSO/EmiMAc (5 vol: 1 vol), proven as a successful solvent for the NMR of cellulose (Gunnarsson et al., 2017; Luo et al., 2009) and measured on Bruker Avance HDIII 800 MHz spectrometer equipped with TXO cryoprobe (Bruker BioSpin GmbH, Rheinstetten, Germany). The ^{13}C spectra were recorded at 298 K using a z-restored spin-echo sequence with a relaxation delay of 3.0 s and a total of 2048 scans and analysed with TopSpin software (v.4.1.1; Bruker BioSpin GmbH, Rheinstetten, Germany).

2.3.3. FTIR spectroscopy

The FTIR spectra were recorded at room temperature (64 scans, 4 cm^{-1} resolution and a 1 cm^{-1} scanning interval) with PerkinElmer Frontier FTRI (Fourier Transform Infrared) spectrometer (PerkinElmer, Llantrisant, UK) equipped with a GladiATR (Attenuated Total Reflectance) sampler (PIKE Technologies, Madison, USA) and PerkinElmer Spectrum software (v. 10.4) in a range 400 to 4000 cm^{-1}. Spectra were baseline-corrected and normalized (1314 cm^{-1} treatment-resistant band of CH_2) (Široký et al., 2010). The original spectra were used to follow the methods of O'connor et al. (1958), Nelson and O'Connor (1964), and Nada et al. (2000) to calculate the Lateral Order Index (LOI), Total Crystallinity Index (TOI) and Hydrogen Bond Intensity (HBI), respectively. The literature-based assignment of the infrared absorbance spectra is summarised in Table A-1 in Supporting Information.

2.3.4. XRD spectroscopy

The high-resolution crystallinity patterns of precipitated samples were obtained using the D8 Advance X-ray diffraction platform (Bruker AXS, Germany) equipped with the dynamic beam optimization and Lynx-eye PSD detector by scanning over the range of 2θ diffraction angle from 5° to 40° using the 0.02° step size (all samples) for Cu Kα radiation (λ = 1.5406 Å), generated at voltage 40 kV and current of 100 mA.

The crystallinity indexes (CIs) were determined by separating the amorphous and crystalline phases from diffracted spectra. For amorphous series, the raw XRD data were Fourier transformed in MATLAB with the predefined fit() command and 8 parameters to determine. For the crystalline series, the backgrounds were firstly subtracted in EVA software (v. 5.2, Bruker AXS, Germany), an approach shown to result in the most accurate model for following deconvolution and crystallinity calculation (Yao et al., 2020). Data were further deconvoluted in the Fityk program (v. 1.3.1, Marcin Wojdyr, Poland) with the R^2 of deconvoluted fitting >0.96 for the applied Voigt function. The areas under the adjusted crystalline (I_C) and amorphous (I_{AM}) peaks were used to calculate CIs according to Eq. (1) (French, 2020; Park et al., 2010; Terinte et al., 2011; Yao et al., 2020), *i.e.*:

$$CI = \frac{I_C}{I_C + I_{AM}} \times 100\% \quad (1)$$

3. Results and discussion

3.1. Behaviour of the CO_2 (g) and cellulose-NaOH(aq) systems at 25 °C

The interactions between NaOH(aq), as well as cellulose-NaOH(aq) and the continuously delivered CO_2(g) at 25 °C, were examined *in-situ* with FTIR, following the pH and temperature change. The process was broken into sections over time, considering the variations between the observed carbonated species, consumption of hydroxide ions (*ergo*, change in pH) and temperature fluctuation, as presented in Fig. 2.

At the beginning of the aeration process, the CO_2(g) was physically absorbed into both systems (Yoo et al., 2013); the process is clearly defined in 3D plots in Fig. 2, highlighted with the darkest colour (for inverted plots, see Fig. A-1 in Supporting Information). Thereafter, in NaOH(aq), the CO_2(aq) almost instantly[1] reacted with OH^-(aq) and generated CO_3^{2-}(aq) ions (Section 1), the rate of which could be observed with the IR at 1380 cm^{-1} (Fig. 2a). The net reaction at this point could be summarised as (Fleischer et al., 1996; Hikita et al., 1976):

$$NaOH_{(aq)}\left\{Na^+_{(aq)} + OH^-_{(aq)}\right\} + CO_{2_{(g)}} \rightarrow Na_2CO_{3_{(g)}}\left\{Na^+_{(aq)} + CO_3^{2-}(aq)\right\} + H_2O_{(aq)} \quad (2)$$

The vast consumption of hydroxide ions and exothermic production of carbonate was characterized by a sharp decrease in the pH and an increase in temperature (Fig. 2a′), demonstrating the dominance of reaction (2) (Yoo et al., 2013). As the formation of CO_3^{2-} reached its maximum, the alkalinity continued to decrease at a slower rate (Section 2, Fig. 2a′), as a consequence of bi-carbonation (reaction (3), accompanied by a steady pH and temperature drop –typical behaviour of an alkaline system saturated with CO_3^{2-}(aq) (Fleischer et al., 1996; Hikita et al., 1976; Yoo et al., 2013).

$$Na_2CO_{3_{(aq)}}\left\{2Na^+_{(aq)} + CO_3^{2-}(aq)\right\} + CO_{2_{(g)}} + H_2O_{(aq)} \rightarrow 2NaHCO_{3_{(aq,s)}} \quad (3)$$

The consumption of CO_3^{2-}(aq) was observed in FTIR spectra (Fig. 2a), characterized by shifting band maxima from 1380 cm^{-1} to 1360 cm^{-1} and the appearance of other peaks characteristic for HCO_3^- *i.e.:* 1308, 1064 and 1008 cm^{-1}, with absorbance trend plotted in Fig. 2a′ (for reference spectra of carbonated species see Fig. A-2 in Supporting Information). Upon the $CO_{3(aq)}^{2-} \rightarrow HCO_{3(aq)}^-$ conversion that finally led to saturation and temperature drop, white crystals appeared. The high concentration of ions (Na^+, CO_3^{2-}, HCO_3^-), H_2O medium and applied temperature could generate an environment favourable for the crystallisation of salt with a rod-like morphology, called "Trona" (Bonfim-Rocha et al., 2020; Clancy et al., 2018; Yoo et al., 2013), *i.e.*:

$$NaHCO_{3(aq)} + Na_2CO_{3_{(aq)}} + 2H_2O_{(aq)} \rightarrow (NaHCO_3 \bullet Na_2CO_3 \bullet 2H_2O)_{(s)} \quad (4)$$

[1] At the high pH, the reaction between $CO_{2(aq)}$ and OH^- is so fast that $CO_{2(g)} \rightarrow CO_{2(aq)}$ conversion can be neglected, and $CO_{2(g)}$ form is used in net reaction, the convention also used herein.

Fig. 3. Pictures of reaction vessels before, during and at the end of the reaction between CO_2(g) and cellulose/NaOH(aq) solution (2 % in 2.0 M, respectively) at 25 °C and 5 °C.

The subsidiary reaction between free Na^+(aq) and HCO_3^-(aq) could give rise to $NaHCO_3$ precipitation (Fleischer et al., 1996; Yoo et al., 2013) resulting in a pH plateau at the end of section 3 (Fig. 2a′).

The response of the cellulose/NaOH(aq) to CO_2(g) aeration was, though, rather different. Specifically, in contrast to the fast pH drop of the reference solvent (by approximately 3 units) in section 1 of cellulose/NaOH(aq) solution, a very modest change by ~0.7 unit (pH 13.8 → 13.1) was observed (Fig. 2b′). Furthermore, the pH drop was accompanied by the precipitation of the gel-like cellulose material (Fig. 3).

The cellulose coagulation from the NaOH (aq) is not unusual, especially if considering the increase of temperature above 20 °C when the7 hydrophobic effect between cellulose chains presumably catalyses the gel compactification (Budtova and Navard, 2016; Cai and Zhang, 2006; Roy et al., 2003). Yet, the process requires long exposure to such temperature (>20 °C), especially at a diluted state (Roy et al., 2003). Here, the precipitation was not only close to instantaneous at surprisingly high pH, but happened upon minimal temperature contribution (Δ ≈ 9 °C) during the exothermic reaction of inorganic carbonate. Moreover, following the absorbance profile of inorganic carbonate (Fig. 2b′), the observed aggregation could be assumed a result of combined factors, *i.e.:* increased temperature and likely the cellulose-mediated chemisorption of CO_2(g), as suggested in previous research (Gunnarsson et al., 2017, 2018, 2020; Wang et al., 2016). In Section 1, the portion of CO_2(g) was most probably 'consumed' by cellulose, whether as a cellulose carbonate intermediate or its hydrolysis product (CO_3^{2-}) captured by the precipitating material; consequently, the reduced rate of gas absorption that led to semi-plateaued FTIR signal was observed during the aggregation (Fig. 2b′). As soon as all cellulose available in the solution precipitated, the entire volume of delivered CO_2(g) could engage in conversion to CO_3^{2-}(aq), thereupon observed as the increase of 1380 cm^{-1} absorption peak in Section 2 (Fig. 2b′).

On the other, after the coagulation of cellulose the system would be expected to behave as a cellulose-free, *ergo*, follow the carbonation trend of the reference solvent (Fig. 2a). Yet, a considerable amount of CO_3^{2-}(aq) has been introduced through the cellulose reaction (Scheme 1), *i.e.*, through a non-alkali-consuming route, bringing the system into an unusual state characterized by both high alkalinity and high CO_3^{2-}(aq) content. Over the Sections 2 and 3, the pH remains high (above 11.9), albeit constantly decreasing: during Section 2 due to the remaining introduction of CO_3^{2-}(aq) through the classical OH^--route until saturation, and during Section 3 under the formation of HCO_3^- (Fig. 2b) finally leading to the salting out of inorganic species visible on the gel surface (Fig. 3). At this point, it would be impossible to decide on the chemical composition of precipitated salt. However, as the pH range at which it precipitated was too low for pure Na_2CO_3 and too high for $NaHCO_3$, it could be assumed to be a mixture of inorganic, carbonate species (trona and bicarbonates) (Atman et al., 1985; Kobe and Sheehy, 1948).

3.2. Behaviour of the CO2 (g) and cellulose-NaOH(aq) systems at 5 °C

The analysis of reaction profiles was repeated for both systems after lowering the temperature to 5 °C. All trends plotted at 5 °C for the reference alkali solvent were principally identical to those at 25 °C. The only exception was a slight delay of the initial dissolution of CO_2(g) in Section 1 ($t_{\text{end zone 1}}$ = 5.17 and 7.10 min respectively; Fig. 4b′ and Fig. 2a′), being the result of the temperature-dependent dissolution limit of CO_3^{2-} (Chesny, 1932; Mun et al., 2018).

Surprisingly, the reaction profiles collected in the presence of cellulose differed drastically from this plotted at 25 °C. The physical absorption of CO_2(g) at 5 °C took a place at the beginning of gas delivery (first 2 min), marked with the darkest colour in the IR plot in Fig. 4b (for inverted plots, see Fig. A-1 in Supporting Information), without considerable change of pH or temperature. Thereafter, the ongoing exothermic conversion of $CO_{2(g)} \rightarrow CO_{3(aq)}^{2-}$ resulted in a temperature jump in Section 1, however, without expected pH drop (Fig. 4b′). Thus, the amount of consumed OH^- in the reaction with CO_2(g) to yield CO_3^{2-} was assumed considerably lower than in the cellulose-free and cellulose-NaOH(aq) solutions at 25 °C. The very modest drop of pH by 0.3 units (pH 14.0 → 13.7) was finally observed at the end of Section 1, resulting in vast precipitation of cellulose gel (Fig. 3); there, the temperature reached maximum (16.5 °C) and started to deplete as soon as gel precipitated (Fig. 4b′). Furthermore, maximum absorbance of CO_3^{2-} was reached, however, without the intensity change of the corresponding band (1380 cm^{-1}) over Section 2 (minimal fluctuations due to measurement and normalization), regardless of the continuous gas delivery. The slowly increasing pH plateaued around 25 min of reaction (Fig. 4b′). The analysis of both pH and IR plateaus in Section 2 of Fig. 4b′ led to the conclusion regarding the saturation of system with CO_3^{2-} at the end of Section 1 and consequent termination of inorganic carbonation. The

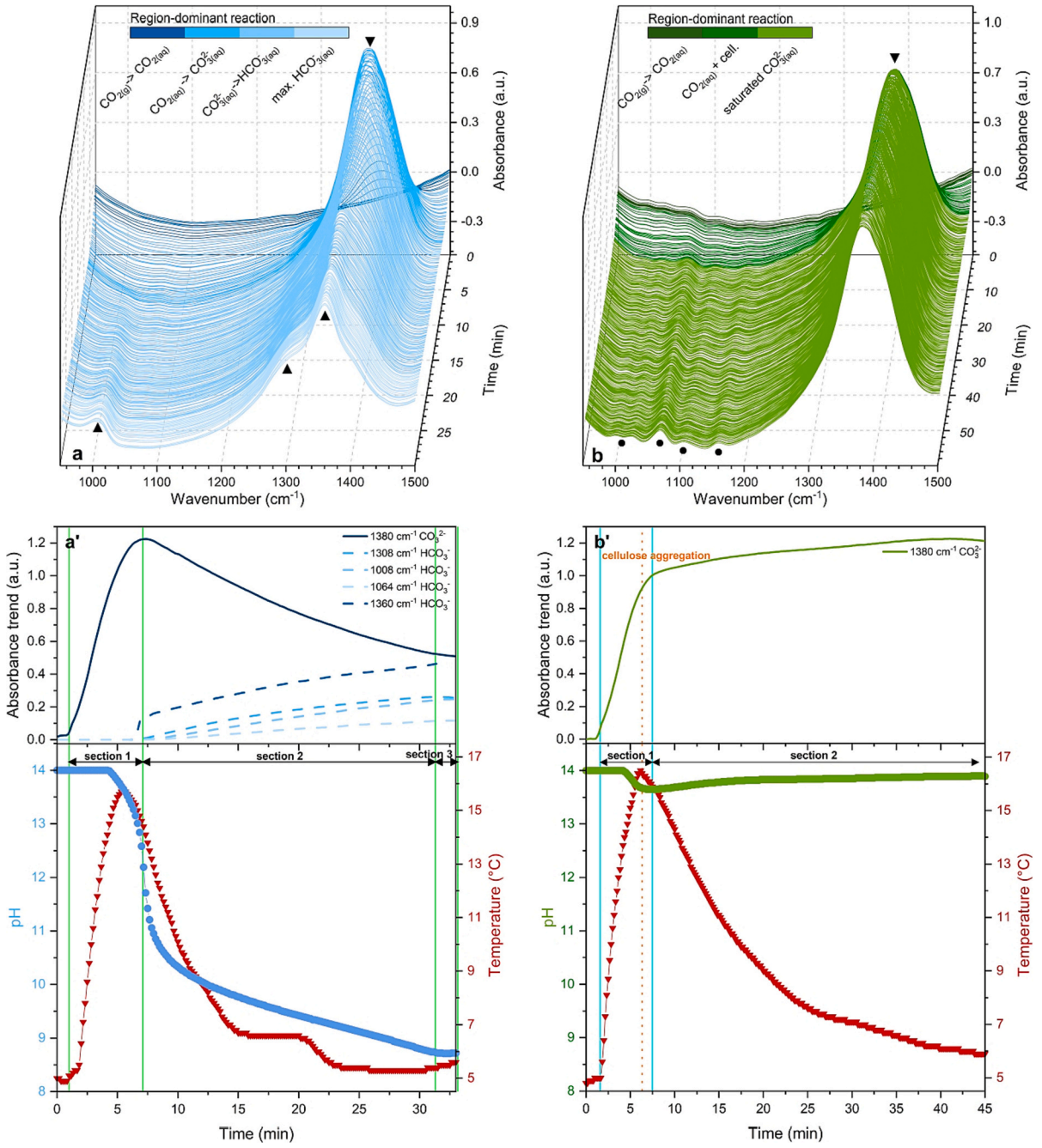

Fig. 4. The FTIR absorbance of carbonate ions, change of pH and temperature, observed during the sparging of CO_2(g) over the a) 2.0 M NaOH and b) cellulose/2.0 M NaOH at 5 °C. Aggregation of cellulose and inorganic salting-out were marked with orange. ▼ – CO_3^{2-} peaks; ▲ – HCO_3^- peaks; ● – cellulose peaks.

precipitation of inorganic salt was either very minor or did not occur at 5 °C (no inorganic crystals noted, Fig. 3), most probably due to the presence of only CO_3^{2-}, the precipitation of which (in form of Na_2CO_3) requires special conditions (Bowman, 2000; Mun et al., 2018). The presence of cellulose most probably enabled saturation with CO_3^{2-} at high pH, blocking the further formation of HCO_3^{2-}.

In accordance with the previously proposed mechanism, introduction of CO_2(g) into the system goes likely *via* a cellulose reaction, kinetically favoured over the reaction with OH^-. During this reaction, cellulose alkoxides are responsible for the actual "incorporation" of CO_2 through a nucleophilic attack converting it – without loss of alkalinity (*i.e.:* consumption of OH^-) – into a transient cellulose carbonate, easily hydrolysed to CO_3^{2-} (Scheme 1). Noteworthy, apart from the early work (Faurholt, 1927; Franchimont, 1910) pointing out incorporation of CO_2(g) into organic carbonates by cellulose analogues in alkaline solutions, a recent work of Gunnarsson et al. showed for the first time spectroscopic evidence of formation of cellulose carbonate from CO_2 (Gunnarsson et al., 2021a; Gunnarsson et al., 2021b). How fast this carbonate hydrolyses into CO_3^{2-}(aq) and how the hydrolysis product contributes to the observed coagulation of cellulose remains to be investigated.

3.3. Comparison of cellulose aggregation at 5 °C and 25 °C and possible reaction mechanism

Looking at such a clear difference between the answer of cellulose/NaOH(aq) to CO_2(g) at 25 °C and 5 °C, the question about the reasons arises immediately. This variation could be associated with depleted

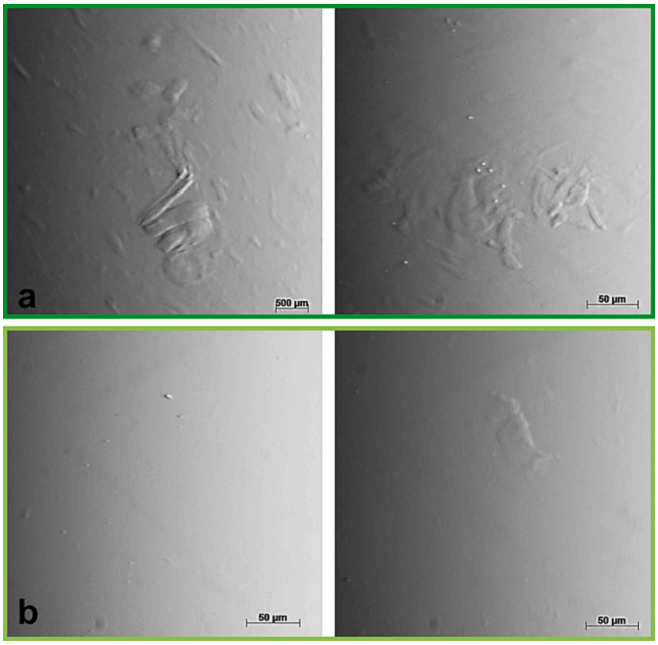

Fig. 5. Microscopic picture of cellulose (2.0 %) dissolved in NaOH (2.0 M, −5 °C) before the CO_2 aeration at a) 25 °C and b) 5 °C. Samples were withdrawn 5 min before the gas delivery, after the temperature stabilization.

stability of cellulose solutions at higher temperatures (Swensson et al., 2020). The microscopy analysis (Fig. 5) confirmed partial spontaneous coagulation of cellulose at 25 °C, while the solution kept at 5 °C remained stable. Consequently, at 25 °C, a less 'properly' dissolved polymer was available in the solution to interact with introduced CO_2(g) resulting only in a partial CO_2-driven aggregation. The increased temperature (weakening H-bonding stabilization and promoting cellulose-cellulose interactions) was partly a driving coagulating force reducing, thus, the possibility of the incoming CO_2(g) to be chemisorbed by the dissolved polymer; especially if considering the temperature inverse solubility of CO_2(g) (Adnan et al., 2020; Lucile et al., 2012; Viadero, 2019). At 5 °C, on the other hand, where the access to the dissolved polymer allowed an efficient chemisorption (Scheme 1), the situation was reversed: the CO_2-driven coagulation was associated with a highly modest alkalinity drop and the CO_3^{2-}saturation of the system prevented any further consumption of OH^- upon prolonged CO_2-areation.

Another question that requires addressing concerns the actual mechanism of observed aggregation. The gelation is considered the effect of ionic strength, composition, pH or temperature amendments leading to a re-assembled polymer network (Cui, 2005; Harding et al., 2017; Lindman et al., 2017; Sun, 2004); with the gelation of cellulose/NaOH(aq) mostly discussed in terms of temperature increase affecting cellulose-cellulose interactions through water exclusion (Budtova and Navard, 2016; Cai and Zhang, 2006; Roy et al., 2003; Swensson et al., 2020). Matter-of-factly, the delivery of CO_2(g) into the system would cause all these changes, ticking all the gelation boxes. Introduction of the anionic organic cellulose carbonate should be particularly considered along with the behaviour of its presumed counterion (Na^+). While the Na^+ is probably too small to support a cation-mediated formation of polysaccharide network (Gurikov and Smirnova, 2018; Sartori, 1997; Tako, 2015), its structure-ordering properties upon hydration with water (Tako, 2015) should be considered pointing out the possibility of coordination with the hydrated carbonate ions. The readily structure-making Na^+ distributed around charged cellulose molecules in the presence of the anionic cellulose carbonate and/or its hydrolysis product (the extremely chaotropic CO_3^{2-} anion) could affect both hydrogen bond network as well as electrostatic interaction.

The uncertain aggregation theory emphasises the need for further study of the subject. For now, given the striking differences in coagulation behaviour at 5 °C and 25 °C, it was highly interesting to further analyse the materials coagulated from both systems.

3.4. Analysis of cellulose material regenerated from CO_2-gels

If the CO_2-driven coagulation of cellulose from NaOH(aq) is to be seen as an alternative in cellulose coagulation technology, it needs to result in the materials at least comparable to those sourced *via* currently available techniques, especially as the prolonged delivery of CO_2(g) entails the risk of incorporation of carbonate species. NMR, ATR-FTIR and XRD showed no structural deviation of CO_2(g) precipitated cellulose from samples precipitated with EtOH (apart from some minor differences in supramolecular order), pointing out that the CO_2-driven aggregation with following aqueous neutralisation could be successfully applied for polymer recovery. The resemblance of 140–170 ppm regions in the NMR spectra (Fig. 6a vs. b & c) confirms the previously suggested reversibility of cellulose carbonation upon H_2O washing (Gunnarsson et al., 2017) and efficient removal of inorganic carbonates, as confirmed by absence of peaks at ~159 ppm (HCO_3^-) and ~166 ppm (CO_3^{2-}) (Abbott et al., 1982; Gunnarsson et al., 2021a; Gunnarsson et al. 2021b).

The change in FTIR absorption bands peaks indicative of conversions from cellulose I to cellulose II (at 3488, 3440 cm^{-1}, 1450–1150 cm^{-1} and 1150–650 cm^{-1}) and those revealing changes in the amorphous regions (2896 → 2891 cm^{-1}) (Carrillo et al., 2004; Oh et al., 2005a; Oh et al., 2005b; Široký et al., 2010) (Fig. 7) were identical after CO_2(g) and EtOH recovery, as well as the 2θ peaks detected by the XRD analysis (Fig. 8) Azubuike et al., 2012; French, 2014; Gong et al., 2017; Nomura et al., 2020). In both cases, the shape of the diffraction pattern suggests an incomplete conversion to cellulose II, which according to the detailed and extensively cited work of French (2014) emphasises the relevance of crystallinity calculations, which brings us to the final section discussed

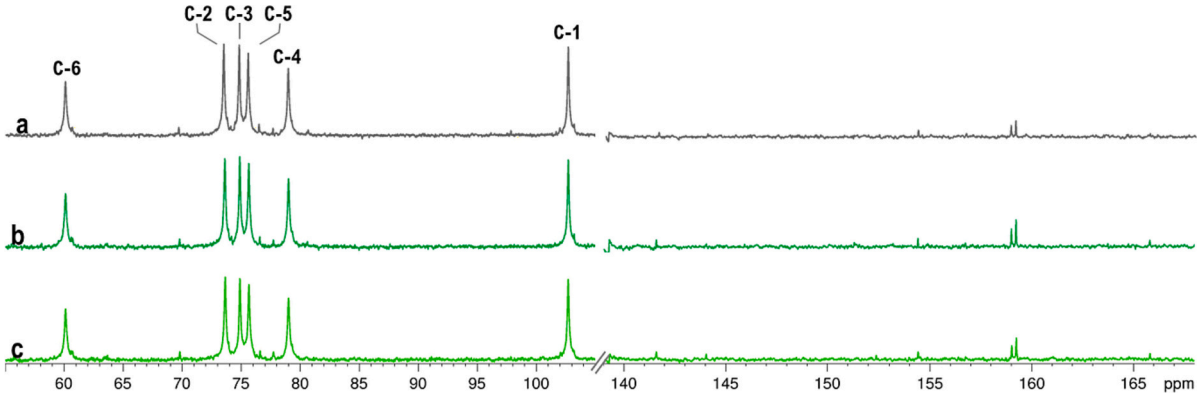

Fig. 6. The ^{13}C NMR spectra of a) MCC standard and cellulose aggregated at b) 25 °C and c) 5 °C from 2.0 M NaOH(aq) by CO_2(g).

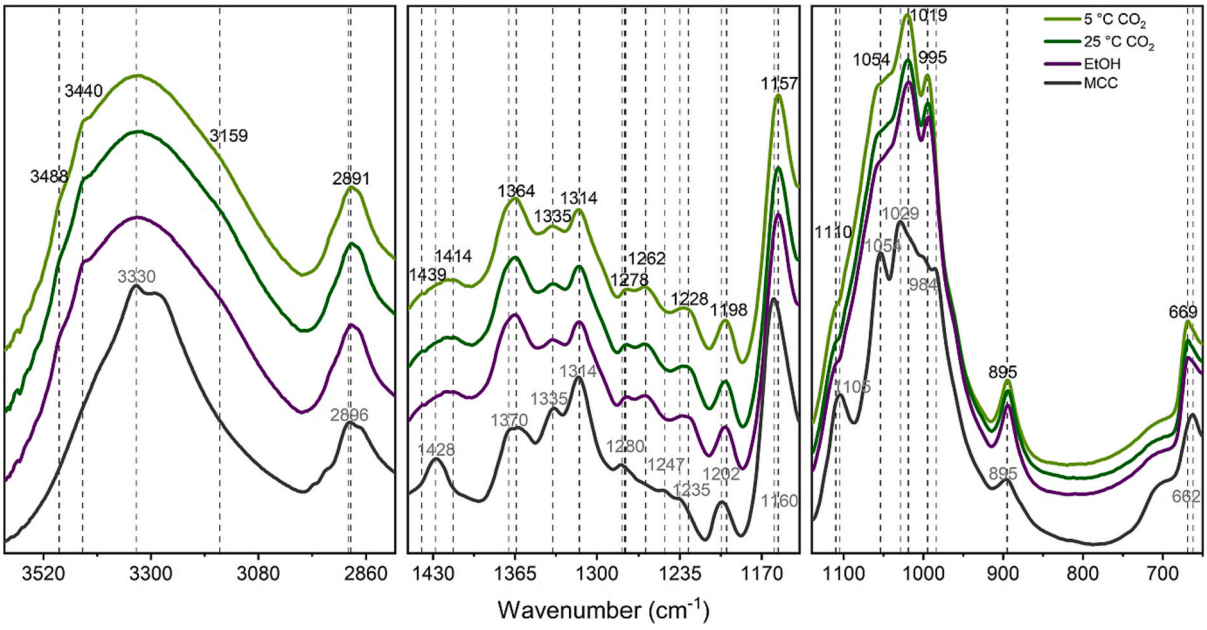

Fig. 7. The FTIR spectra (3600–600 cm^{-1}) for MCC standard and MCC precipitated from NaOH(aq) (2 % in 2.0 M, respectively) with EtOH (RT), CO_2 at 25 °C and CO_2 at 5 °C.

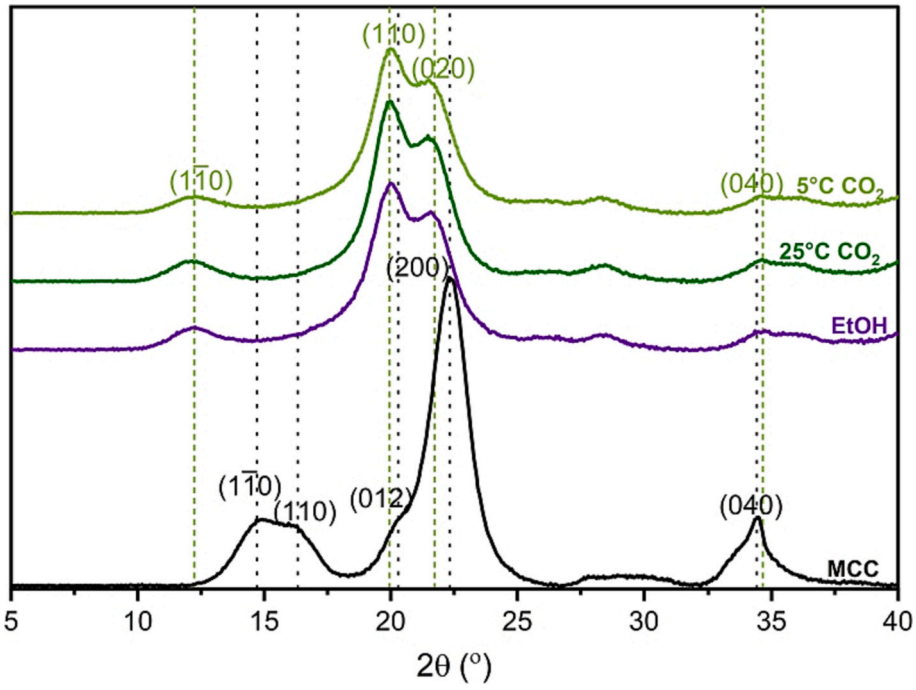

Fig. 8. The XRD patterns of cellulose precipitated from 2.0 M NaOH(aq) with EtOH (RT), and CO_2 at 25 °C and 5 °C, plotted against the MCC standard.

in this work.

Based on FTIR data the lateral order index (LOI), total crystallinity index (TCI) (Nelson and O'Connor, 1964; O'Connor et al., 1958;) and hydrogen bond intensity (HBI) (Nada et al., 2000) were calculated, while portions of crystalline and amorphous regions were estimated *via* XRD data (Fig. 9) based on deconvoluted diffraction patterns (Fig. A-3, Supplementary Information).

The cellulose I to cellulose II transformation caused by NaOH(aq) treatment resulted in lower LOI values in general that differed with respect to the recovery method as follows: $LOI_{EtOH} < LOI_{25°C\ CO2} < LOI_{5°C\ CO2}$ (Fig. 9). The TCI presented parallel to LOI behaviour, elegantly underlying the cellulose I → cellulose II transformation (Fig. 9). Lastly, the hydrogen-bond effect could be summarised in $HBI_{EtOH} > HBI_{25°C\ CO2} > HBII_{5°C\ CO2}$ order.

The EtOH-recovery of cellulose from NaOH(aq) resulted, evidently, in the material of increased crystallinity and reinforced order, sustained by a strong hydrogen network; the characteristic typical for cellulose precipitated from moderately concentrated NaOH (≤10 %) with a polar medium (Nomura et al., 2020; Oh et al., 2005a; Oh et al., 2005b; Široký et al., 2010). The crystallinity obtained by CO_2-percipitation was comparable. However, the effect of hydrogen bonding was diminished, especially at 5 °C (Fig. 9), which possibly points out towards

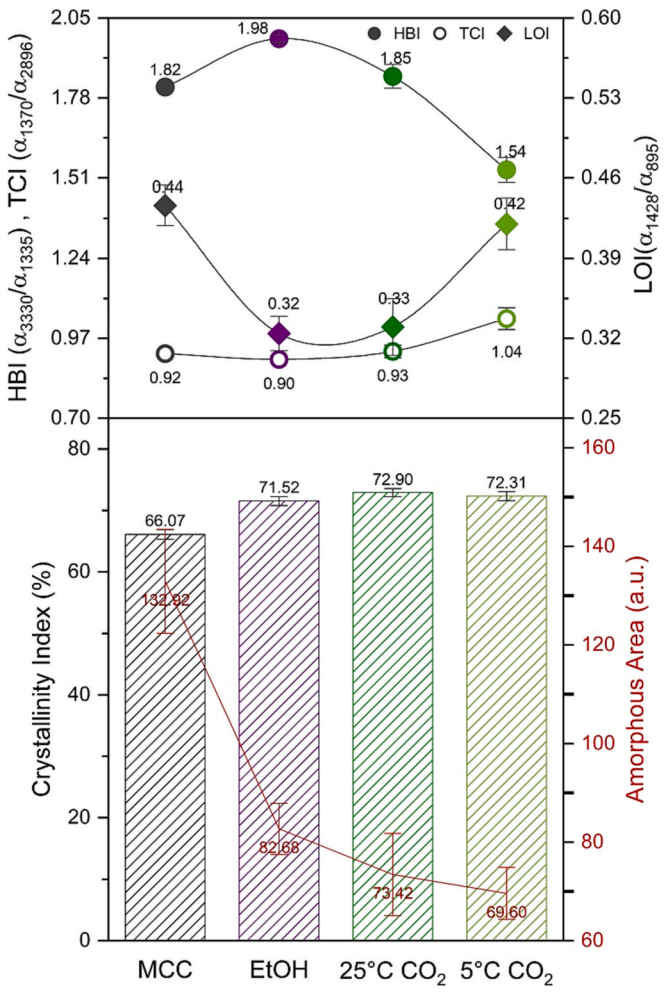

Fig. 9. The crystallinity of MCC standard and cellulose precipitated from 2.0 M NaOH(aq) with EtOH (RT), CO_2 at 25 °C and 5 °C. The upper plot shows data calculated using the FTIR spectra. The lower plot summarises calculations through deconvolution of XRD data.

contribution of carbonate species (introduced through mediation of cellulose) in the coagulation mechanism promoting the possibility of stacking the chains, leaving the door open for further studies.

4. Conclusions

The coagulant action of CO_2(g) accomplishes an efficient and highly alkali-preserving precipitation of cellulose provided the conditions (*i.e.* temperature and dissolved state of cellulose) allow for an efficient cellulose-mediated chemisorption of the introduced CO_2(g). The minimum alkalinity loss during coagulation particularly boosts the attractiveness of the process from the implementation perspective, as it opens up for a highly resource efficient recycling of the solvent/coagulation bath (apart from utilizing one of the cheapest and most available gases). With the perspective for future applications, this research opens the door to following studies on cellulose-CO_2 based materials.

CRediT authorship contribution statement

Aleksandra M. Kozlowski: Conceptualization, Methodology, Visualization, Writing – original draft, Validation. **Merima Hasani:** Conceptualization, Resources, Supervision, Writing – review & editing, Validation.

Declaration of competing interest

The authors declare that they have no known competing financial interests or personal relationships that could have appeared to influence the work reported in this paper.

Data availability

Data will be made available on request.

Acknowledgements

This work has been funded by the Åforsk Research Foundation (Stockholm, Sweden). The authors acknowledge Michal Strach (Chalmers Materials Analysis Laboratory, CMAL) for help with XRD analysis and Shirin Naserifar for introduction to FTIR. The Swedish NMR Center is acknowledged for the spectrometer time.

Appendix A. Supplementary data

Supplementary data to this article can be found online at https://doi.org/10.1016/j.carbpol.2022.119771.

References

Abbott, T. M., Buchanan, G. W., Kruus, P., & Lee, K. C. (1982). 13 C nuclear magnetic resonance and Raman investigations of aqueous carbon dioxide systems. *Canadian Journal of Chemistry, 60*(8), 1000–1006. https://doi.org/10.1139/v82-149

Adnan, A. I., Ong, M. Y., Nomanbhay, S., & Show, P. L. (2020). Determination of dissolved CO2 concentration in culture media: Evaluation of pH value and mathematical data. *Processes, 8*(11), 1–15. https://doi.org/10.3390/pr8111373

Atman, G., Tuncer, S., & Gungor, N. (1985). Remarks on different methods for analyzing trona and soda samples. *Bulletin of the Mineral Research and Exploration Institute of Turkey, 105*, 57–67.

Azubuike, C. P., Rodríguez, H., Okhamafe, A. O., & Rogers, R. D. (2012). Physicochemical properties of maize cob cellulose powders reconstituted from ionic liquid solution. *Cellulose, 19*(2), 425–433. https://doi.org/10.1007/s10570-011-9631-y

Benedetti-Pichler, A. A., Cefola, M., & Waldman, B. (1939). Warder's method for the titration of carbonates. *Industrial and Engineering Chemistry - Analytical Edition, 11*(6), 327–332. https://doi.org/10.1021/ac50134a012

Bergenstråhle, M., Wohlert, J., Himmel, M. E., & Brady, J. W. (2010). Simulation studies of the insolubility of cellulose. *Carbohydrate Research, 345*(14), 2060–2066. https://doi.org/10.1016/j.carres.2010.06.017

Bonfim-Rocha, L., Silva, A. B., De Faria, S. H. B., Vieira, M. F., & De Souza, M. (2020). Production of sodium bicarbonate from CO2 reuse processes: A brief review. *International Journal of Chemical Reactor Engineering, 18*(1), 1–16. https://doi.org/10.1515/ijcre-2018-0318

Bowman, 2000 R. W. Bowman (2000). Process for the Manufacture of Sodium Carbonate Crystals from Minerals or Solutions. (Patent No. 6,022,385).

Budtova, T., & Navard, P. (2016). Cellulose in NaOH–water based solvents: A review. *Cellulose, 23*(1), 5–55. https://doi.org/10.1007/s10570-015-0779-8

Cai, J., & Zhang, L. (2006). Unique gelation behavior of cellulose in NaOH/urea aqueous solution. *Biomacromolecules, 7*(1), 183–189. https://doi.org/10.1021/bm0505585

Carrillo, F., Colom, X., Suñol, J., & Saurina, J. (2004). Structural FTIR analysis and thermal characterisation of lyocell and viscose-type fibres. *European Polymer Journal, 40*(9), 2229–2234. https://doi.org/10.1016/j.eurpolymj.2004.05.003

Chesny, 1932. H. Chesny (1932). Process of precipitating sodium bicarbonate from solutions in form of coarse crystals (Patent No. US1865832A).

Clancy, D., Patel-Jones, J., & Hutton, G. (2018). Accelerated stability modeling: Investigation of disintegration time of a drug product with sodium bicarbonate. In *Accelerated predictive stability* (pp. 403–410). Elsevier. https://doi.org/10.1016/B978-0-12-802786-8.00019-X. Issue 1.

Cui, S. W. (2005). Food carbohydrates: chemistry, physical properties, and applications. In *Food carbohydrates* (1st ed.). Taylor & Francis Group, LLC.

Cuissinat, C., & Navard, P. (2008). Swelling and dissolution of cellulose, part III: Plant fibres in aqueous systems. *Cellulose, 15*(1), 67–74. https://doi.org/10.1007/s10570-007-9158-4

Darmana, D., Henket, R. L. B., Deen, N. G., & Kuipers, J. A. M. (2007). Detailed modelling of hydrodynamics, mass transfer and chemical reactions in a bubble column using a discrete bubble model: Chemisorption of CO2 into NaOH solution, numerical and experimental study. *Chemical Engineering Science, 62*(9), 2556–2575. https://doi.org/10.1016/j.ces.2007.01.065

Egal, M., Budtova, T., & Navard, P. (2007). Structure of aqueous solutions of microcrystalline cellulose/sodium hydroxide below 0 °C and the limit of cellulose dissolution. *Biomacromolecules, 8*(7), 2282–2287. https://doi.org/10.1021/bm0702399

Egal, M., Budtova, T., & Navard, P. (2008). The dissolution of microcrystalline cellulose in sodium hydroxide-urea aqueous solutions. *Cellulose, 15*(3), 361–370. https://doi.org/10.1007/s10570-007-9185-1

Faurholt, C. (1927). Studies on monoalkyl carbonates. II. The formation of monoalkyl carbonic acids or their salts on dissolving carbon dioxide in aqueous solutions of alcohols of different degrees of acidity. *Zeitschrift für Physikalische Chemie B, 126*, 85–104.

Fleischer, C., Becker, S., & Eigenberger, G. (1996). Detailed modeling of the chemisorption of CO2 into NaOH in a bubble column. *Chemical Engineering Science, 51*(10), 1715–1724. https://doi.org/10.1016/0009-2509(96)00030-9

Franchimont, A. P. N. (1910). On sodium-alkyl carbonates. In , *12. KNAW Proceedings* (pp. 303–304).

French, A. D. (2014). Idealized powder diffraction patterns for cellulose polymorphs. *Cellulose, 21*(2), 885–896. https://doi.org/10.1007/s10570-013-0030-4

French, A. D. (2020). Increment in evolution of cellulose crystallinity analysis. *Cellulose, 27*(10), 5445–5448. https://doi.org/10.1007/s10570-020-03172-z

Goharrizi, A. S., & Abolpour, B. (2014). Modeling an industrial sodium bicarbonate bubble column reactor. *Applied Petrochemical Research, 4*, 235–245. https://doi.org/10.1007/s13203-014-0064-z

Gong, J., Li, J., Xu, J., Xiang, Z., & Mo, L. (2017). Research on cellulose nanocrystals produced from cellulose sources with various polymorphs. *RSC Advances, 7*(53), 33486–33493. https://doi.org/10.1039/c7ra06222b

Gunnarsson, M., Theliander, H., & Hasani, M. (2017). Chemisorption of air CO2 on cellulose: An overlooked feature of the cellulose/NaOH(aq) dissolution system. *Cellulose, 24*(6), 2427–2436. https://doi.org/10.1007/s10570-017-1288-8

Gunnarsson, M., Bernin, D., Östlund, Å., & Hasani, M. (2018). The CO2 capturing ability of cellulose dissolved in NaOH(aq) at low temperature. *Green Chemistry, 20*(14), 3279–3286. https://doi.org/10.1039/c8gc01092g

Gunnarsson, M., Bernin, D., & Hasani, M. (2020). The CO2/CO32−chemistry of the NaOH(aq) model system applicable to cellulose solutions. *Cellulose, 27*(2), 621–628. https://doi.org/10.1007/s10570-019-02782-6

Gunnarsson, M., Bernin, D., & Hasani, M. (2021a). On the interference of urea with CO2/CO32- Chemistry of cellulose model solutions in NaOH(aq). *Carbohydrate Polymers, 251*(August 2020), Article 117059. https://doi.org/10.1016/j.carbpol.2020.117059

Gunnarsson, M., Bernin, D., Hasani, M., Lund, M., & Bialik, E. (2021b). Direct evidence for reaction between cellulose and CO 2 from nuclear magnetic resonance. *ACS Sustainable Chemistry & Engineering, 9*(42), 14006–14011. https://doi.org/10.1021/acssuschemeng.1c05863

Gurikov, P., & Smirnova, I. (2018). Non-conventional methods for gelation of alginate. *Gels, 4*(1), 14. https://doi.org/10.3390/gels4010014

Harding, S. E., Tombs, M. P., Adams, G. G., Paulsen, B. S., Inngjerdingen, K. T., & Barsett, H. (2017). *An introduction to polysaccharide biotechnology*. Issue 4 (2nd ed.) (2nd ed.,. *80*. CRC Press. https://www.taylorfrancis.com/books/9781482248326 https://www.taylorfrancis.com/books/9781482248326.

Hikita, H., Asai, S., & Takatsuka, T. (1976). Absorption of carbon dioxide into aqueous sodium hydroxide and sodium carbonate-bicarbonate solutions. *The Chemical Engineering Journal, 11*(2), 131–141. https://doi.org/10.1016/S0300-9467(76)80035-4

Kobe, K., & Sheehy, T. (1948). Thermochemistry of sodium carbonate and it's solutions. *Industrial & Engineering Chemistry, 40*(12). https://doi.org/10.1021/ie50468a600, 2370-2370.

Lindman, B., Karlström, G., & Stigsson, L. (2010). On the mechanism of dissolution of cellulose. *Journal of Molecular Liquids, 156*(1), 76–81. https://doi.org/10.1016/j.molliq.2010.04.016

Lindman, B., Medronho, B., Alves, L., Costa, C., Edlund, H., & Norgren, M. (2017). The relevance of structural features of cellulose and its interactions to dissolution, regeneration, gelation and plasticization phenomena. *Physical Chemistry Chemical Physics, 19*(35), 23704–23718. https://doi.org/10.1039/c7cp02409f

Lucile, F., Cézac, P., Contamine, F., Serin, J., Houssin, D., & Arpentinier, P. (2012). Solubility of carbon dioxide in water and aqueous solution containing sodium hydroxide at temperatures from (293.15 to 393.15) K and pressure up to 5 MPa: Experimental measurements. *Journal of Chemical & Engineering Data, 57*(3), 784–789. https://doi.org/10.1021/je200991x

Luo et al., 2009 M. Luo A. N. Neogi H. West (2009). Dissolution of cellulose in mixed solvent system (Patent No. US20090084509A1).

Medronho, B., & Lindman, B. (2015). Brief overview on cellulose dissolution/regeneration interactions and mechanisms. *Advances in Colloid and Interface Science, 222*, 502–508. https://doi.org/10.1016/j.cis.2014.05.004

Mun, S. J., Han, S. J., & Wee, J. H. (2018). Carbon dioxide fixation by precipitating NaHCO3 via carbonation of NaOH-dissolved ethanol aqueous solution. *Energy and Fuels, 32*(8), 8614–8622. https://doi.org/10.1021/acs.energyfuels.8b01584

Nada, A.-A. M. A., Kamel, S., & El-Sakhawy, M. (2000). Thermal behaviour and infrared spectroscopy of cellulose carbamates. *Polymer Degradation and Stability, 70*(3), 347–355. https://doi.org/10.1016/S0141-3910(00)00119-1

Nelson, M. L., & O'Connor, R. T. (1964). Relation of certain infrared bands to cellulose crystallinity and crystal lattice type. Part II. A new infrared ratio for estimation of crystallinity in celluloses I and II. *Journal of Applied Polymer Science, 8*(3), 1325–1341. https://doi.org/10.1002/app.1964.070080323

Nomura, S., Kugo, Y., & Erata, T. (2020). 13C NMR and XRD studies on the enhancement of cellulose II crystallinity with low concentration NaOH post-treatments. *Cellulose, 27*(7), 3553–3563. https://doi.org/10.1007/s10570-020-03036-6

O'sullvian, A. C. (1997). Cellulose: The structure slowly unravels. *Cellulose, 4*(3), 173–207. https://doi.org/10.1023/A:1018431705579. https://doi.org/10.1023/A:1018431705579

O'connor, R. T., Dupré, E. F., & McCall, E. R. (1958). Applications of infrared absorption spectroscopy to investigations of cotton and modified cottons: Part II: Chemical modifications. *Textile Research Journal, 28*(7), 542–554. https://doi.org/10.1177/004051755802800702

Oh, S. Y., Yoo, D. I., Shin, Y., Kim, H. C., Kim, H. Y., Chung, Y. S., … Youk, J. H. (2005a). Crystalline structure analysis of cellulose treated with sodium hydroxide and carbon dioxide by means of X-ray diffraction and FTIR spectroscopy. *Carbohydrate Research, 340*(15), 2376–2391. https://doi.org/10.1016/j.carres.2005.08.007

Oh, S. Y., Yoo, D. I., Shin, Y., & Seo, G. (2005b). FTIR analysis of cellulose treated with sodium hydroxide and carbon dioxide. *Carbohydrate Research, 340*(3), 417–428. https://doi.org/10.1016/j.carres.2004.11.027

Park, S., Baker, J. O., Himmel, M. E., Parilla, P. A., & Johnson, D. K. (2010). Cellulose crystallinity index: Measurement techniques and their impact on interpreting cellulase performance. *Biotechnology for Biofuels, 3*(1), 10. https://doi.org/10.1186/1754-6834-3-10

Roy, C., Budtova, T., Navard, P., & Bedue, O. (2001). Structure of cellulose-soda solutions at low temperatures. *Biomacromolecules, 2*(3), 687–693. https://doi.org/10.1021/bm010002r

Roy, C., Budtova, T., & Navard, P. (2003). Rheological properties and gelation of aqueous cellulose−NaOH solutions. *Biomacromolecules, 4*(2), 259–264. https://doi.org/10.1021/bm020100s

Saberi, A., Goharrizi, A. S., & Ghader, S. (2009). Precipitation kinetics of sodium bicarbonate in an industrial bubble column crystallizer. *Crystal Research and Technology, 44*(2), 159–166. https://doi.org/10.1002/crat.200800429

Sartori, C. (1997). *The characterisation of alginate systems for biomedical applications (Issue May)*. Brunel University. http://bura.brunel.ac.uk/handle/2438/7399.

Schönherr, J., Buchheim, J. R., Scholz, P., & Adelhelm, P. (2018). Boehm titration revisited (part I): Practical aspects for achieving a high precision in quantifying oxygen-containing surface groups on carbon materials. *Journal of Carbon Research, 4*(2), 21. https://doi.org/10.3390/c4020021

Shim, J. G., Lee, D. W., Lee, J. H., & Kwak, N. S. (2016). Experimental study on capture of carbon dioxide and production of sodium bicarbonate from sodium hydroxide. *Environmental Engineering Research, 21*(3), 297–303. https://doi.org/10.4491/eer.2016.042

Sipos, P., May, P. M., & Hefter, G. T. (2000). Carbonate removal from concentrated hydroxide solutions. *Analyst, 125*(5), 955–958. https://doi.org/10.1039/a910335j

Široký, J., Blackburn, R. S., Bechtold, T., Taylor, J., & White, P. (2010). Attenuated total reflectance Fourier-transform infrared spectroscopy analysis of crystallinity changes in lyocell following continuous treatment with sodium hydroxide. *Cellulose, 17*(1), 103–115. https://doi.org/10.1007/s10570-009-9378-x

Sun, S. F. (2004). Physical chemistry of macromolecules. In *Basic principles and issues* (2nd ed.). John Wiley & Sons Inc.

Swensson, B., Larsson, A., & Hasani, M. (2020). Dissolution of cellulose using a combination of hydroxide bases in aqueous solution. *Cellulose, 27*(1), 101–112. https://doi.org/10.1007/s10570-019-02780-8

Tako, M. (2015). The principle of polysaccharide gels. *Advances in bioscience and biotechnology, 06*(01), 22–36. https://doi.org/10.4236/abb.2015.61004

Tepe, J. B., & Dodge, B. F. (1943). Absorption of carbon dioxide by sodium hydroxide solutions in a packed column. *Transactions of the Institution of Chemical Engineers, 39*, 255–276.

Terinte, N., Ibbett, R., & Schuster, K. C. (2011). Overview on native cellulose and microcrystalline cellulose I structure studied by X-ray diffraction (WAXD): Comparison between measurement techniques. *Lenzinger Berichte, 89*, 118–131.

Viadero, R. (2019). Principles of gas solubility in water: Henry's law. In *Encyclopedia of water* (pp. 1–7). Wiley. https://doi.org/10.1002/9781119300762.wsts0096. Issue 3.

Wang, J., Xue, Z., Yan, C., Li, Z., & Mu, T. (2016). Fine regulation of cellulose dissolution and regeneration by low pressure CO2 in DMSO/organic base: Dissolution behavior and mechanism. In , *Vol.18. Physical Chemistry Chemical Physics* (pp. 32772–32779). https://doi.org/10.1039/c6cp05541a. Issue 48.

Yao, W., Weng, Y., & Catchmark, J. M. (2020). Improved cellulose X-ray diffraction analysis using Fourier series modeling. *Cellulose, 27*(10), 5563–5579. https://doi.org/10.1007/s10570-020-03177-8

Yoo, M., Han, S. J., & Wee, J. H. (2013). Carbon dioxide capture capacity of sodium hydroxide aqueous solution. *Journal of Environmental Management, 114*(November), 512–519. https://doi.org/10.1016/j.jenvman.2012.10.061

Zhang, L., Ruan, D., & Gao, S. (2002). Dissolution and regeneration of cellulose in NaOH/thiourea aqueous solution. *Journal of Polymer Science Part B: Polymer Physics, 40*(14), 1521–1529. https://doi.org/10.1002/polb.10215